Personalized ventilation solutions for reducing CO2 levels in the crew quarters of the International Space Station

M.R. Georgescu, Amina Meslem, I. Nastase, F. Bode

Building and Environment 204 (2021) 108150

Contents lists available at ScienceDirect

Building and Environment

journal homepage: www.elsevier.com/locate/buildenv

Personalized ventilation solutions for reducing CO_2 levels in the crew quarters of the International Space Station

Matei Razvan Georgescu [a,b,*], Amina Meslem [a], Ilinca Nastase [b], Florin Bode [b,c]

[a] University of Rennes, LGCGM, 3 Rue du Clos Courtel, BP 90422, 35704, Rennes, CEDEX 7, France
[b] CAMBI Research Center, Technical University of Civil Engineering of Bucharest, 66 Pache Protopopescu Boulevard, 021414, Bucharest, Romania
[c] Technical University of Cluj-Napoca, Mechanical Engineering Department, B-dul Muncii nr. 103-105, D03, 400641, Cluj-Napoca, Romania

ARTICLE INFO

Keywords:
ISS ventilation
CO_2 accumulation in microgravity
Human breathing modelling
Breathing zone air quality
Lobed air diffuser
CFD

ABSTRACT

The present paper studies the possibility of personalized ventilation (PV) systems to improve air quality in the breathing zone of astronauts resting in the crew quarters aboard the International Space Station. In the absence of gravity CO_2 accumulates in pockets near the astronaut's head, potentially leading to symptoms of CO_2 intoxication. The addition of a PV system aimed at an astronaut's breathing zone during sleep could provide a supply of fresh air directly to the face and reduce the risks of intoxication. Experimental measurements of the PV diffuser velocity fields were performed in an experimental setup and the results were used to validate the numerical solution for the PV case connected to the already existing general ventilation system of the crew quarters. CFD models were used in order to reproduce the conditions of microgravity. Two PV configurations were studied, the first with the PV diffuser position in front of the human occupant and the second was positioned laterally, both being aimed at the breathing zone. The results were compared to a case without PV. Results indicate that the lateral PV solution is more viable than the frontal solution providing a reduction in overall CO_2 levels in the breathing zone. The lateral PV also leads to an 8% reduction in the volume of CO_2 inhaled over the course of each breath having the potential to improve air quality over longer periods of time.

1. Introduction

The present study showcases personalized ventilation (PV) solutions adapted to the environment of the astronaut crew quarters (CQ) aboard the International Space Station (ISS) with the aim of reducing CO_2 accumulation around the head by supplying fresh air to the breathing zone (BZ) of the occupants.

Carbon dioxide accumulation is a known problem aboard spacecraft [1–4] as in the absence of gravity, exhaled CO_2 gathers in pockets around the human head if the ventilation conditions are not adequate, such as in confined spaces. The astronaut CQ is such a confined space where the astronauts store their personal belongings and where they sleep [4]. The CQ are a later addition to the ISS (sent in 2008) and as such, each of them has a separate ventilation system [4,5]. The ventilation system uses two axial fans to supply airflow to the interior of the CQ. The two axial fans are mounted in series to guard against the eventuality than one fan breaks down while the astronauts are sleeping inside the CQ – as without a second fan, such a situation could pose a significant asphyxiation hazard for the occupants [3–5]. The CQ ventilation circuit is covered in sound-proofing materials and follows an intricate trajectory from the inlets on the ISS corridor to the diffuser grille inside the CQ [5–7]. The fan rotation speed can be varied to supply one of the three fixed airflow rates (108, 138 and 156 m^3/h) [5].

Regardless of the above-mentioned measures to combat CO_2 accumulation in the CQ, several issues arise. Despite the CQ design fulfilling its design criteria (from a ventilation and acoustic point of view) [7], reports indicate that the ventilation system could be improved [5,6]. Firstly, when the fans are set to the lowest flow rate (108 m^3/h) reports indicate [5,6] that the fan failure alarm occasionally goes off, attributing this fact to the continuous accumulation of dust in the CQ ventilation system, which, by introducing head losses, decreases the flow rate supplied by the fans to the point that the alarm is set off. Increasing the flow rate alleviates this problem, but on the highest fan setting (156 m^3/h) noise complaints have been filed [5].

Because of these limitations, situations arise when the ventilation systems are not able to effectively combat CO_2 accumulation, as

* Corresponding author. 66 Pache Protopopescu boulevard, 021414, Romania.
E-mail addresses: mateirazvangeorgescu@gmail.com (M.R. Georgescu), amina.meslem@univ-rennes1.fr (A. Meslem), ilinca.nastase@utcb.ro (I. Nastase), florin.bode@termo.utcluj.ro (F. Bode).

https://doi.org/10.1016/j.buildenv.2021.108150
Received 22 April 2021; Received in revised form 7 July 2021; Accepted 13 July 2021
Available online 15 July 2021

evidenced by astronaut reports [3,4,7] of occasional symptoms of CO_2 intoxication. Attempts have been made [1,8,9] to establish limits of CO_2 concentration after which would prevent the phenomenon of CO_2 intoxication from occurring. But the fact that common environmental CO_2 concentration aboard the ISS is high (3000–6500 ppm [8] as opposed to ~400 ppm at sea level on Earth) as a limitation of the Environmental Control and Life Support System's energy requirements [8,10,11], coupled with the high degree in personal tolerance to CO_2 between individuals [8,9,12] makes establishing such a theoretical limit almost as difficult as obtaining it in practice with the current technological advances. The conclusion of the reports evaluating the crew's susceptibility to CO_2 intoxication was to keep the CO_2 levels as low as possible.

When considering the confined nature of the CQ and the limitations of its ventilation system, an idea emerged that CO_2 intoxication symptoms could be alleviated if a part of the CQ's ventilation were targeted on the BZ of the occupant via a personal ventilation (PV) system. This would allow the removal of CO_2 from around the occupant's head where it accumulates during sleep [2,11,13,14]. For the implementation of a PV system, the existing ventilation circuit needs to be altered and the region of CO_2 accumulation needs to be accurately identified. Previous work [15] has established the region of CO_2 accumulation in the CQ in the absence of ventilation, as an approximately 4 cm wide and extending up to 11 cm in front of the occupant's nose. This zone, termed as the BZ showed an increased concentration of CO_2 without gravitational acceleration [15] caused by the lack of a convective boundary layer around the occupant in this case. For the present study, the BZ will be targeted by the PV solution. The modification of the ventilation system consists in simplifying the ventilation circuit and replacing the previous two axial fans with cross-flow fans providing less energy consumption and improved acoustic parameters for the same flow parameters [16,17]. The question that remains to be answered is what kind of PV solution should be used to ventilate the BZ?

Cleaner air in the BZ mandates a certain degree of control over the flow features of the BZ. On Earth, one must also contend with the free convection flow of the human boundary layer. Any attempt at supplying a fresh flow of air to the BZ via PV needs to either penetrate this boundary layer (i.e., velocities over 0.3 m/s) or make the PV flow more independent of its surroundings. Observations are that the PV flow strongly interacts with the convective boundary layer of the human body [18].

PV designs such as furniture incorporated air diffusers (in tables or chairs) [19] or air terminal devices (ATDs) [20] are usually situated away from occupant's breathing zone. Attempts have been made to dissipate the boundary layer through forced ventilation [21] or to diminish the strength of its flow by cooling the desk where the occupant is seated [22] in the hopes of improving PV efficiency. Results indicated improved levels of clean air for the occupant using reduced PV airflow (25% less), i.e., the weakening of the convective boundary layer reduced required PV airflow from 8 L/s to 6 L/s.

Additional PV diffusers in conjunction with several ATDs [20] installed in the headrest of a chair can weaken the convective boundary layer and increase clean air percentage. This method provided 30% more clean air in the BZ with a flow rate of 4 l/s. Using low PV flow rates is a possible as long as the convective boundary layer can be sufficiently weakened. This way, PV can be used even by people sensitive to air draft.

Another method to improve PV performance is to reduce the distance between the occupant and the PV diffuser [23,24]. This can lower the PV flow rates to as little as 0.5 L/s resulting in most of the air inhaled (>90%) being clean air. Other factors that influence this approach are the initial velocity, equivalent diameter of the diffuser as well as its geometry [25].

Lobed orifices in a perforated panel ceiling diffuser can be used in mixing ventilation to improve initial jet spread due to increased induction, without reducing the jet's throw length [26,27]. The lobed edges of the diffuser nozzle cause the formation of large stream-wise structures known to improve the jet induction phenomenon [28,29]. Lobed diffuser nozzles were also found to have a wider initial spread at the cost of increased mixing in comparison to free circular jets or plane jets [29,30]. If the lobed diffuser were situated close to the face, the initial spread would be an asset because the PV jet would cover more of the occupant's BZ, but would not have time to mix with the polluted air inside the CQ due to the short distance. Two lobed diffuser geometries were investigated [31]: a six-lobed hemispherical nozzle and a 4-lobed clover-like hemispherical nozzle. The six-lobed diffuser was compared well in performance to circular and elliptical diffuser at 0.04 m and 0.06 m from the mouth at a velocity of 0.4 m/s.

If air is diffused in proximity of an occupant's face, the inserted flow should not affect the body's thermal sensation [23]. Local discomfort is likely if the initial velocity is high. Experiments evaluating the performance of a rectangular diffuser incorporated in a headset [32] with an initial velocity of around 1.7 m/s were met with reports of unpleasant sensations from the human test subjects. Velocities had to be diminished around three times (~0.6 m/s) to reduce the unpleasant sensations of draft [33]. These results [32,33] indicate that velocity values below 0.6 m/s provide acceptable occupant comfort levels at face level.

PV diffusers in proximity of the human face also reduce the exposure of the eyes to the flow of fresh air, if the PV can target the occupant's breathing zone, which is rarely the case when the distance between the head and the PV diffuser is significant and in which case an increased frequency of eye blinking has been reported [34].

In the present case, due to the lack of gravity, the convective boundary layer is practically non-existent, diminishing the previously mentioned difficulties and improving the chances of devising an efficient PV solution. Considering the above-mentioned results, the decision was made for the present study to utilize a six-lobed PV diffuser situated in proximity to the occupant at a distance of 0.06 m (equivalent to $2D_e$, as seen in previous studies [31]). This PV diffuser geometry and distance will enable the PV jet to supply fresh air to a wider region around the face and possibly even compensating small changes in the head's position during sleep (the CQ occupants sleep in a sleeping-bag fixed to the wall, limiting their movement). The aim of the present paper is the study of the efficiency of such a PV diffuser in reducing CO_2 accumulation in the BZ when positioned frontally and laterally near the face of the occupant in comparison to a case where no PV system is utilized. Numerical simulations of the PV system will be validated through experimental results obtained on Earth in an isothermal environment to mimic the lack of buoyancy on the ISS. The gravitational acceleration will then be deactivated in the numerical model in order to simulate the conditions of the ISS environment.

2. Experimental setup

As previously mentioned, the installation of a PV solution in the CQ requires modifying the general ventilation system. An alternative ventilation solution consisting in replacing the axial fans with cross-flow fans (CFF) was studied [17] consisting in replacing the axial fan circuit with a CFF version (Fig. 1), which houses the fans in the upper and lower plenums of the CQ. The CFF solution (Fig. 1) frees up space previously used for ducting and allows the mounting of the PV system in the upper plenum of the CQ, without modifying its structure. The CFF operating curves were experimentally measured and imposed as boundary conditions in CFD models [17]. Comparisons with previously validated airflow fields of the axial fan solution [16] showed the CFF solution to provide improved acoustic and ventilation performance for the same energy consumption. The PV solution will be built around these results.

The PV circuit is connected to the plenum in which the cross-flow fan is mounted, being supplied by the same air which is introduced in the CQ by the general ventilation diffuser grille. As previously mentioned, the PV opening is a six-lobed diffuser with an equivalent diameter $D_e = 3$ cm, offering better initial spread without reducing the jet throw length

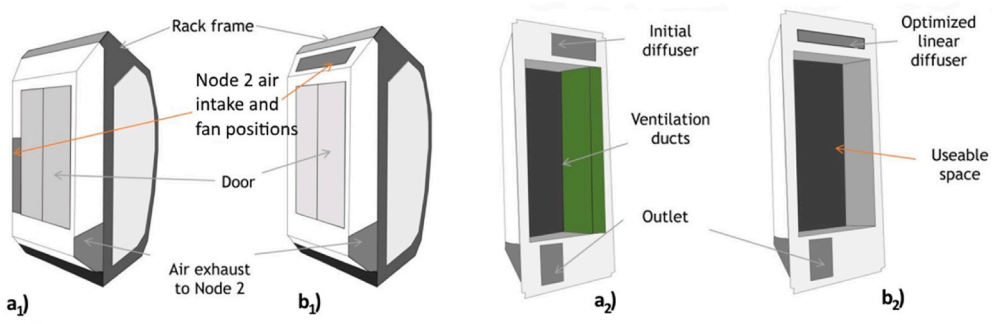

Fig. 1. Schematic representation of the current CQ ventilation solution using axial fans (a_1, a_2) and the alternate ventilation solution using cross-flow fans (b_1, b_2).

[26,27]. The distance between the nozzle and the face of the astronaut is 2De, chosen to enable the usage of low flow rates through the PV circuit.

The flow rate was determined by installing the PV system in the same experimental setup used to study the cross-flow fans [17]. The personalized ventilation circuit was mounted perpendicular to the direction of the airflow provided by the cross-flow fan (the most disadvantaged mounting position) inside the experimental setup. A TSI 4000 Series flow meter, with a measurement range of 0–300 l/min ±2% of reading and a response time of ~4 ms, was installed along the PV circuit. The measured flow rate was stable at 20 l/min, equivalent to 1.2 m3/h.

The PV system was studied by experimentally measuring velocity flow fields at different distances in front of the PV diffuser (0.5, 1 and 1.5 De). Measurements were made using Dantec Dynamics ComfortSense Mini 54N95 fitted with a 54T33 omnidirectional anemometer with a measurement range of 0.05–5 m/s and an accuracy of ±2% or ±0.02 m/s, in the temperature range of −20 °C–80 °C. The diameter of the 54T33 anemometer is 3 mm. The probe was mounted on a 3D automated traverse system, controlled from a nearby computer. The measurement planes were situated at the three above-mentioned distances in front of the diffuser, between it and a humanlike manikin, which was placed in order to reproduce the jet impact phenomenon $2D_e$ in front of the PV diffuser.

The traverse system controlled the positioning of the anemometer in this plane and measurements were made in a 30 × 30 grid (Fig. 2b) extending 6 cm vertically and horizontally from the center of the PV diffuser (so a spatial resolution of 2 mm). Velocity results per point were the averaged velocity values measured in that point for a time period of 30s. The experimental setup is presented in Fig. 2 showing an image of the PV diffuser and the human manikin (a) and a detailed schematic of the entire setup including dimensions and measurement equipment (b). The tachometer and micromanometer shown in Fig. 2b were used in the previous evaluation of the cross-flow fans [17] and were kept for monitoring purposes. The resulting velocity fields of the PV diffuser jet will be used to validate CFD results of the PV flow.

3. Numerical simulation

3.1. Overview of the CFD study

The present study makes extensive use of CFD methods, through the ANSYS Fluent software, for the study of the PV system. The geometrical models are based on the existing design of the CFF general ventilation solution [17] with the PV circuit added in two different configurations: (1) frontal PV emplacement (Fig. 3a) at $2D_e$ in front of the occupant's nose and (2) with the PV placed laterally (Fig. 3b) at the same distance of $2D_e$ from the face. The frontal PV solution, in addition to the study of the PV system itself, will be used to validate the CFD model's ability to reproduce the PV diffuser jet development by comparing it with the experimental velocity field measurements.

For reasons of computational efficiency, the numerical study will use a previously studied methodology [16,17] of simulating the ventilation circuit (called ventilation models - VM, in the present paper) without the occupant in the CQ by imposing the CFF operating curves as boundary conditions and thus obtaining velocity profiles at the diffuser grille and the PV duct connected to the plenum. The velocity profiles are then exported as boundary conditions in what are termed simplified models (SM) which lack the ventilation circuit behind the plenum, but feature the human occupant of the CQ. Separating the problems is necessary because the study of the PV influence on CO_2 accumulation is a complex process that is simulated in a transient state, and available computational resources do not permit (or are rather very inefficient) at solving both the ventilation and the CO_2 accumulation problems at once. The current numerical setup proposes a comparison of 3 cases (No PV, frontal PV and lateral PV) implying the usage of 6 CFD models in total. The relation of these models with each other has been presented in the diagram of Fig. 4 for clarifying the relationship between these cases. From here on the Ventilation models will be termed VM with a number associated (1, 2 and 3 for the no-PV, frontal PV and lateral PV cases respectively). In a similar fashion the simplified models (where the actual evaluation of the PV system will take place) will be termed

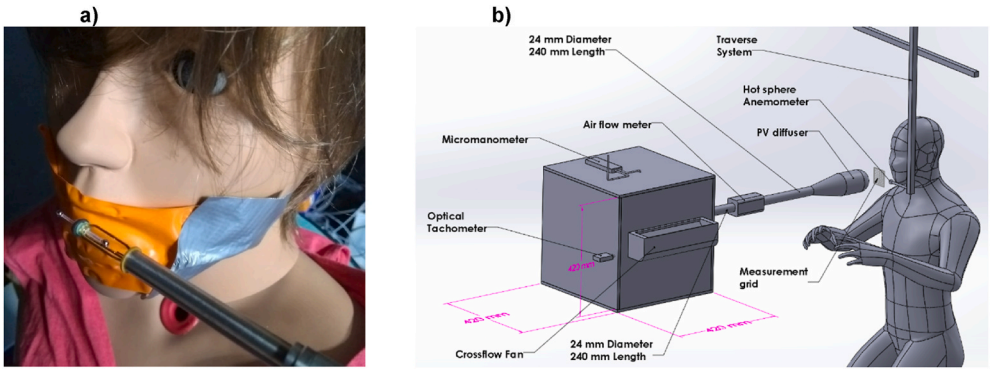

Fig. 2. Experimental setup for measuring the PV airflow velocity in front of a humanlike manikin (a) and its schematic representation (b).

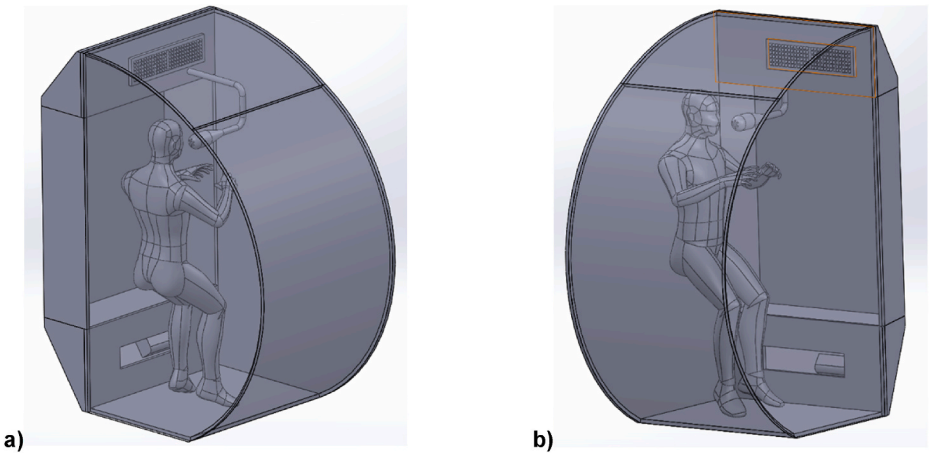

Fig. 3. *Interior view of the CQ featuring the emplacement of the (a) frontal and (b) lateral PV* solutions.

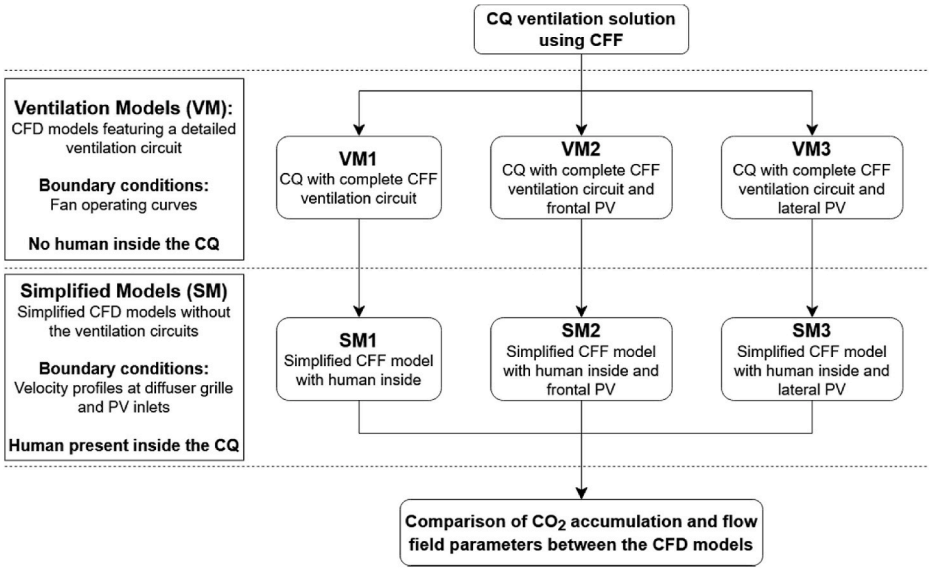

Fig. 4. Workflow of the six CFD models employed in the evaluation of the general and PV ventilation systems as well as the accumulation of CO_2 in the CQ.

SM1-SM3 (Fig. 4).

3.2. Computational grids

The design criteria used for all of the above computational grids were the following: (1) a wall $Y^{+}\sim = 1$, (2) average orthogonal quality above 0.9 and (3) at least five cells in the boundary layer. For all cases the computational grids were generated with tetrahedral cells which were subsequently converted to polyhedral cells in the CFD software to reduce computational demand. Computational grids of several sizes were tested in order to find the ones which were able to accurately describe the flow rate through the fan for the VM cases, and the human breath for the SM cases respectively. The resolutions of the computational grids used in this study are presented in Table 1.

Mesh sections of models VM3 and SM3 (lateral PV) are shown in Fig. 5. The VM numerical grids as a general rule are a bit coarser than their SM counterparts, but sufficiently fine to accurately represent the velocity profiles that need to be extracted from the VM models. For brevity, only the mesh details of VM3 and SM3 are presented.

3.3. Boundary conditions

The VM models used the CFF operating curve as a boundary condition (Fig. 6a). The CFF flow rate for VM1-3 determined at the diffuser was ~140 m^3/h. The diffuser velocity distribution for each VM (Fig. 6b) was used as an inlet boundary condition in its SM counterpart. The PV solution slightly alters the flow rate through the system in VM2 and VM3 because the PV circuits modify the head losses in the circuit. The PV flow rate for VM2 is 1 m^3/h. The flow rate through the lateral PV diffuser (VM3) was initially slightly higher than for the frontal PV diffuser, with lower flow rates through the diffuser grille. Head losses in

Table 1
Computational domain cell count for the six numerical models (VM1-3 and SM1-3).

CFD model parameters	VM1	VM2	VM3	SM1	SM2	SM3
Mesh pre-conversion tetrahedral cell count	~7.5 million	~9 million	~ 10 million	~ 10 million	~ 11 million	~14 million
Mesh post-conversion polyhedral cell count	~2.7 million	~3.3 million	~4 million	~3 million	~4.2 million	~5.5 million

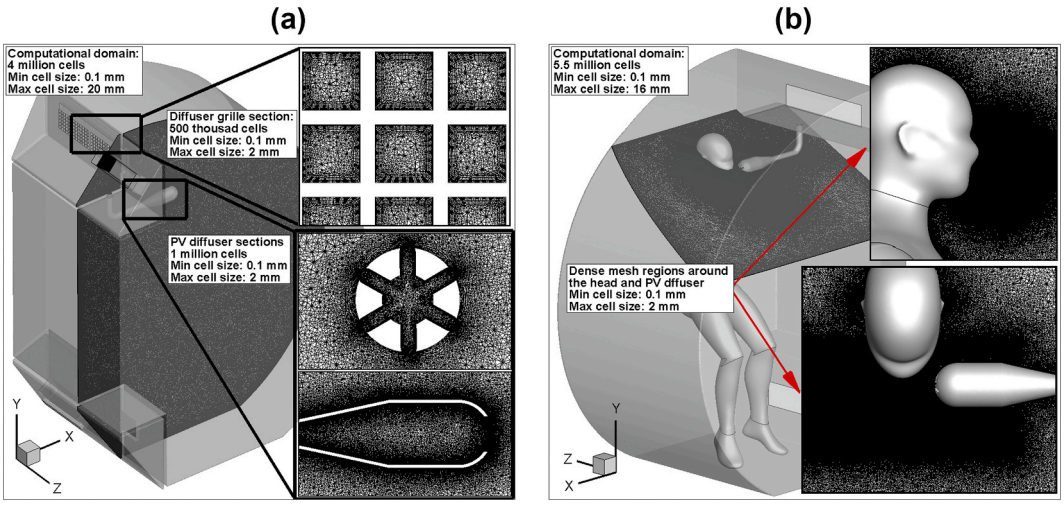

Fig. 5. CFD model mesh for VM3 (a) and SM3 (b) with mesh details highlighting sensitive flow areas such as the diffuser grille, the PV diffuser and the human face.

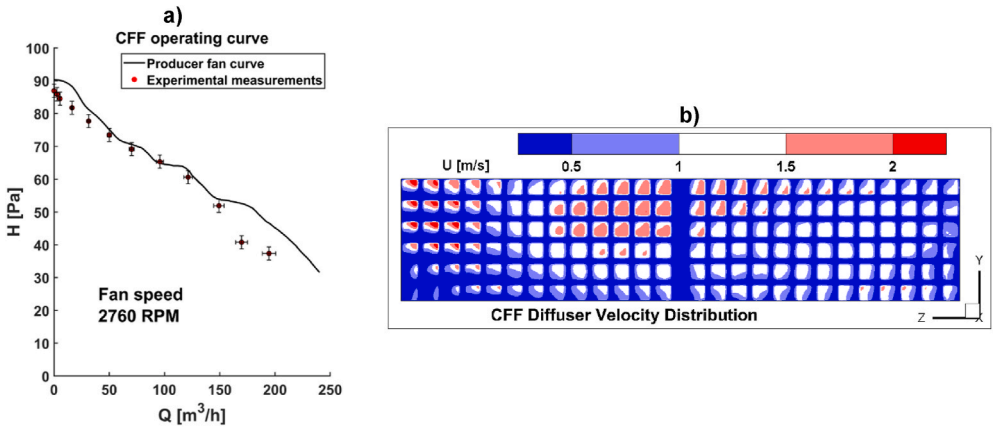

Fig. 6. Experimentally determined CFF operating curve used as a boundary condition in VMs (a); Diffuser velocity distribution used as a boundary condition in SMs (b).

the form of porous zones were introduced on the lateral circuit to keep the two PV solutions at the same flow rate of 1 m^3/h. The remainder of the flow in this case was redistributed through the general ventilation grille and the overall flow rate through the fan change was below 2% and thus considered to have remained constant at ~140 m^3/h.

A turbulence model was required for the CFD simulations as the different inlets have Reynolds numbers ranging from 1200 (PV system) to 12000 (diffuser grille). The turbulence model used for these studies was k-w SST as RANS models have been studied to be well suited to the ISS environment [14,35,36], and because in this case it proved to better represent the PV jet development [37].

Species transport was modelled to reproduce the CO_2 distribution in the CQ. The human occupant in SM1-SM3 was the main source of CO_2, breathing was simulated through a previously studied sine function of the velocity [15] which proved to accurately represent experimental measurements of CO_2 accumulation in an experimental CQ model [15]. This user defined velocity function for the occupant is the equivalent of a pulmonary ventilation rate of 8.5 l/min [15]. Species, velocity and temperature boundary conditions for the occupant and the ambient air are presented in Table 2. All inlet boundary conditions had a turbulence intensity of 5%.

The VM simulations were performed in a steady state. The SM models, because of the variable nature of the human breath, had to be run in a transient state using Unsteady RANS methods. The SM models were run for a total of 60s with a time step of 0.05s, saving data every second time step (so every 0.1s). These parameters have been used in a previous study of the occupant CO_2 generation in the CQ and were found to adequately represent CO_2 accumulation over 60s as measured in an experimental setup [15].

Table 2
Boundary conditions for the human breath, and temperature conditions of the walls and the human body.

	Boundary condition	T [°C]	O_2 volume fraction [−]	CO_2 volume fraction [−]	H_2O volume fraction [−]	Velocity [m/s]
Ambient air	N/A	23	0.21 (21%)	0.0004 (0.04%)	0.0244 (2.44%)	N/A
Nostrils during exhalation	Velocity inlet	36	0.15 (15%)	0.04 (4%)	0.0615 (6.15%)	$u = 5.49 \cdot \sin(2\pi \cdot 0.245 \cdot t)$
Nostrils during inhalation	Velocity inlet	Ambient values				$u = 5.49 \cdot \sin(2\pi \cdot 0.245 \cdot t)$

Wall and human body surface temperatures

Region	Walls	Head	Torso	Arms	Forearms	Hands	Lower abdomen and thighs	Shins	Feet
T [°C]	23	36	34.5	33	32	30	32.5	30	29

4. Results and discussion

4.1. Experimental validation of numerical results

During the experimental measurements, velocity magnitude (V_m [m/s]) fields of the PV jet were measured with a hot-sphere anemometer at three distances in front of the PV diffuser: $0.5D_e$, $1D_e$ and $1.5D_e$ (Fig. 7a, b and c respectively). The measured velocity fields are centered on the PV jet and were measured in a 6 × 6 cm grid with a measurement resolution of 2 mm (31 × 31 measurement points). Results show that the lobed form of the PV jet is clearly seen at $0.5D_e$. At $1D_e$ remnants of the lobed jet are still present, while at $1.5D_e$ those same remnants have almost disappeared as the lobed jet transitions into a round jet. Peak velocities at all three distances (Fig. 7 a-c) are around 0.5 m/s. The jet expands from its width and height (WxH) of approximately 4 × 4 cm at $0.5D_e$ to a WxH of 5 × 5 cm at $1.5D_e$ (an increase of 20%).

The experimental results presented in Fig. 7 are compared to the CFD results of Fig. 8. The aim is to verify that the CFD method can reproduce the development of the lobed jet. For this purpose, the CFD case used was a special case of SM2 (human present, frontal PV) where both the human breath and the general ventilation were deactivated (so as to not influence the PV jet – as per the experimental measurements), and the PV flow rate (CFD) was set to equal that of the experimental setup (1.2 m^3/h). The resulting PV velocity fields at 0.5, 1 and 1.5 D_e are presented in Fig. 8 a-c, respectively. The CFD results are more clearly defined as expected due to their increased resolution (approximately 100 × 100 cells for each velocity field).

The CFD maximum velocity at each distance is around 0.5 m/s although slightly over-estimated by the numerical results, compared to the experimental measurements. The maximum V_m values up to $2D_e$ are plotted in Fig. 8d alongside experimental values. Fig. 8d confirms the numerical overestimation of the maximum V_m, although the overestimation appears to be constant (~0.06 m/s in each case). For further validation, the trajectory of the jet along the X and Y axes up to $2D_e$ in front of the PV diffuser was traced in Fig. 8e and f respectively. The CFD and experimental jet trajectories along the X and Y axes are in good agreement, mostly presenting small differences (<2 mm), with the exception of a divergence along the X axis (~4 mm) at 1.5D (Fig. 8e). The stronger deviation along the X axis represents the jet swerving around the human face. Anything less than perfect alignment between the PV jet and the center of the human face will necessarily cause the jet to slightly prefer swerving either to the right or to the left side of the face. For the CFD model, this swerve is to the right side of the human face (increasing X values) while for the experimental measurements a downward tendency (decreasing X values) indicates that the swerve is slightly to the left explaining the divergence seen in Fig. 8e.

The similarity of the velocity fields between numerical and experimental results, coupled with the good correspondence of the jet maximum velocity as well as the jet trajectories (taking into account the swerve effect along the X axis), lends confidence in the ability of the CFD method to represent the PV jet development to an adequate degree.

4.2. Personalized ventilation implementation

The present study deals with three different CFD cases (SM1-SM3), each with its own peculiarities in regard to the ventilation configuration (presence and orientation of the PV system), and each aiming to study at the same time the effectiveness of the ventilation system and the reduction of CO_2 accumulation in the BZ. The multitude of interactions imposes difficulties upon finding a one-size-fits-all region of comparison for the three models (SM1-SM3). Consequently, three planes of comparison will be investigated (Fig. 9a), each being relevant to the peculiarities of the ventilation system of one CFD case. Thus, the three planes are: (1) the ventilation plane (VP) – relevant for the general ventilation flow supplied by the diffuser grille, selected such that it does not intersect the PV systems or the human inside the CQ in either of the SM cases; (2) the breathing plane (BP) – perpendicular to the nostrils of the human, and consequently the main direction of the breath, while at the same time being relevant for the study of the lateral PV solution (SM3) and the BZ; (3) the median plane (MP) – the median plane of the human body, serves in studying the frontal PV solution (SM2) and the BZ.

The investigations took place at one of the time instants defined as t_1-t_4 and shown in Fig. 9b_1-b_4. These time instants correspond to key moments in the breathing cycle: the peak of the exhalation (t_1); the end of the exhalation (t_2), the peak of the inhalation (t_3) and the end of the inhalation (t_4).

We first investigate if the introduction of the PV system and its position significantly alters the flow fields inside the CQ. Fig. 10 shows velocity fields in the VP of each case (SM1 (a), SM2 (b) and SM3 (c)). The velocity magnitude fields between the three cases are practically unchanged, despite the introduction of the PV system. For case SM2 a protuberance is seen at the top of the stagnant zone in the middle of the CQ, attributed to the downward duct of the frontal PV system influencing airflow in that area, but otherwise no significant change is noted. The results indicate that the PV system has negligible impact on the CQ's general ventilation system, and its introduction is unlikely to change the existing design criteria.

The introduction of the PV system in close proximity to the human, increases the risk of generation of an uncomfortable sensation of draft for the occupant if the velocities exiting the PV diffuser are too high, or if the temperature of the PV air is too low or any combination of the two. The criteria which measures human susceptibility to the draft effect is the Draft Rate (DR [%]) [38,39] which measures the amount of people (in %) which would report an uncomfortable sensation of draft. The DR is calculated by the following equation (1):

$$DR = (34 - T) \cdot (V_{avg} - 0.05)^{0.62} \cdot (0.37 \cdot V_{avg} \cdot T_u + 3.14) \quad (1)$$

Where T is the local air temperature [°C]; V_{avg} is the average local velocity magnitude [m/s] and T_u is the local air turbulent intensity [%]. EN ISO 7730 [38] defines three comfort levels when evaluating the DR: level A (DR<10%), level B (DR<20%) and level C (DR<30%). DR values above 30% are considered uncomfortable and should be avoided in designing ventilation systems.

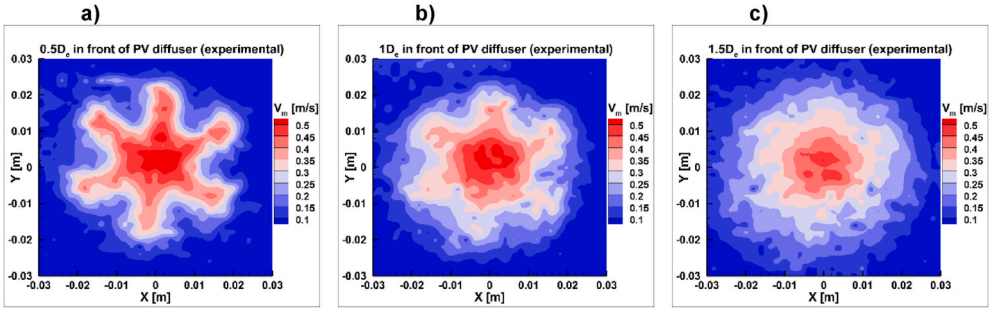

Fig. 7. Velocity fields measured by an omnidirectional hot sphere anemometer at three distances: $0.5D_e$ (a), $1D_e$ (b) and $1.5D_e$ (c).

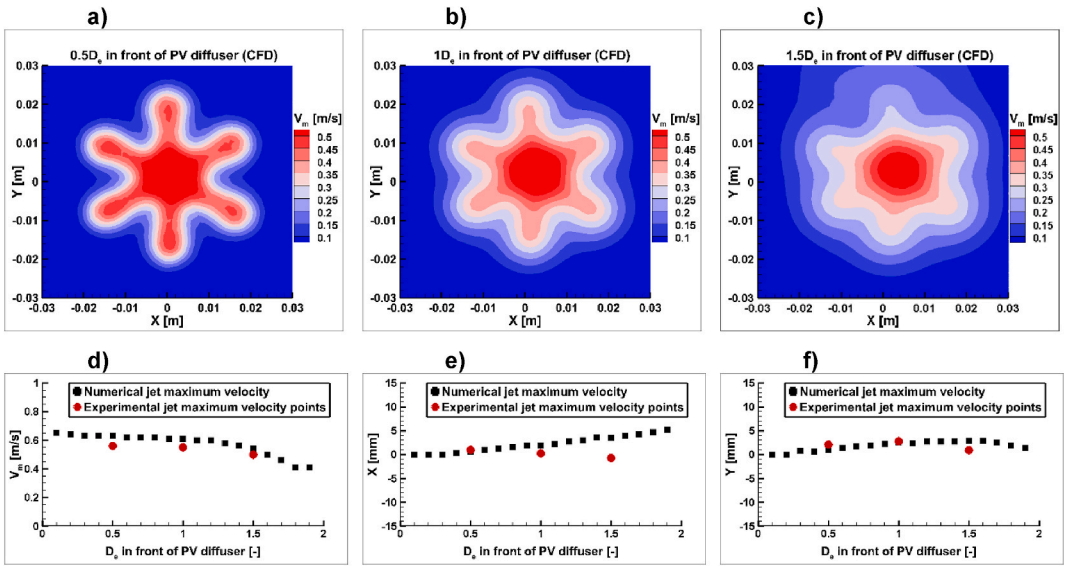

Fig. 8. Validation of the PV system: velocity magnitude at $0.5D_e$ (a), $1D_e$ (b), $1.5D_e$ (c); comparison of the PV jet velocity decay along the Z axis (d); comparison of the experimental and numerical PV jet trajectory along the X axis (e) and the Y axis (f).

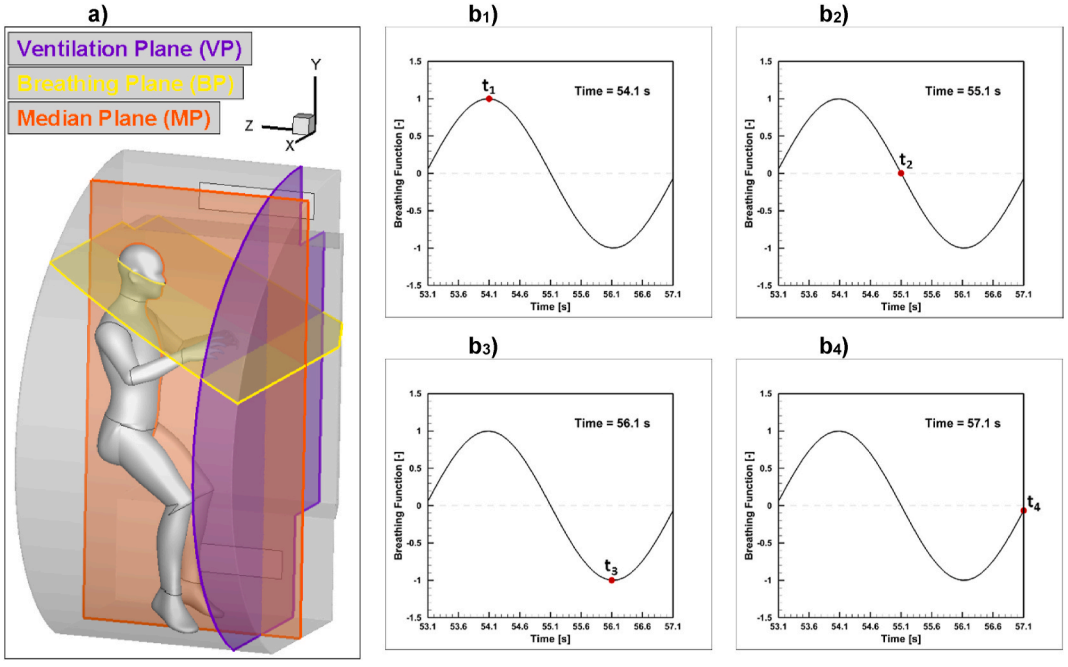

Fig. 9. CFD planes for investigating the flow features of the CQ: one plane for the general ventilation (VP), and two planes for the breathing zone (BP and MP).

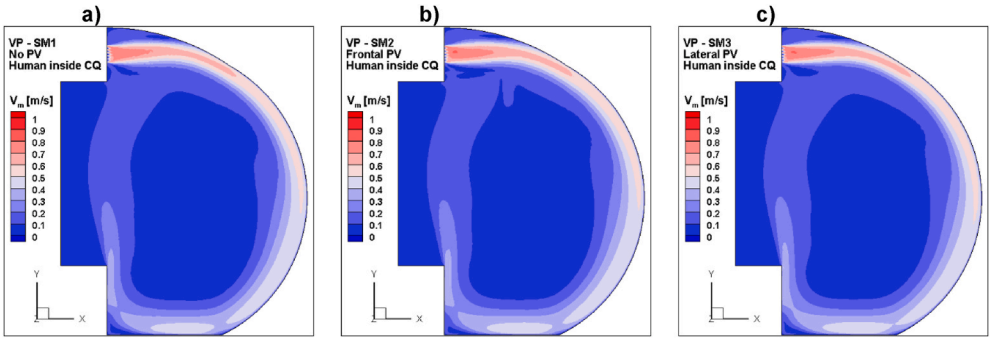

Fig. 10. Comparison of velocity fields in the ventilation plane (VP) for the three simplified CFD models: SM1 (a), SM2 (b) and SM3 (c).

Although Equation (1) was determined on Earth, microgravity conditions should not affect its viability for assessing occupant draft sensations. At most it would alter the importance of certain parameters in the equation (turbulent intensity and temperature) as discussed below.

In the absence of gravity, the flow is largely unaffected by temperature differences. A consequence of this fact is the absence of the human convective boundary layer which in turn causes a reduction in turbulent intensity around the human body. In Fig. 11 the T_u fields are presented for SM1 (a), SM2 (b) and SM3 (c). Turbulent intensity values around the human body are mostly around 5% for the three cases. The exception is the frontal PV case which presents higher turbulent intensity around the nose and mouth of the occupant most likely due to the direct impact of the frontal PV jet (Fig. 11b). This phenomenon is not present in the lateral PV case (Fig. 11c).

Despite the lack of the convective boundary layer, temperature still plays an important role in DR determination through the first term of Equation (1). Concerning the present case, temperatures on the ISS modules vary between 18 and 27 °C [1,3,10] (most of the time, the temperature on the modules is around 23 °C [5,7]). For evaluating the DR in the present case (Fig. 11) the worst-case temperature scenario was considered where the ambient air has a temperature of 18 °C and the ventilation flow from the PV system and the diffuser is also supplied at 18 °C.

Fig. 11 shows DR fields for SM1 (d), SM2 (e) and SM3 (f) in their respective evaluation planes (Fig. 9a). Following the EN ISO 7730 [38] comfort classification regarding the DR we see that most of the CQ falls in the Class A comfort level, with the head and feet of the occupant being situated in a class B comfort zone for the cases with PV. Class C comfort zones are found near the feet of the occupant and in front of the nose in the case of the lateral PV solution. This is the expected behavior as the PV jet has higher velocities than most of the CQ volume. Areas of unacceptable DR (over 30%) are found near the diffuser grille and along the curved wall, as well as right at the exit of the PV diffuser.

4.3. PV efficiency in CO_2 removal

Because the PV solutions do not significantly impact the comfort of the occupant, the study proceeds with the investigation of the CO_2 accumulation in the CQ for the three cases (SM1-SM3). The first evaluation criterion is the average CO_2 accumulation in the entire CQ volume. Previous work [15] has highlighted an increase in the CQ of the CO_2 level without ventilation. The purpose here is to see if the general ventilation and PV systems can combat the phenomenon of accumulation and if the answer is "yes" to identify to what degree this take place. Fig. 12 shows the evolution of the average concentration of CO_2 [ppm] in the CQ over 20 s. The last 20s of the 60s simulation were chosen because in the first half of the simulation the general ventilation and PV flows have yet to stabilize and thus the results could be misleading.

In Fig. 12 we can see that the accumulation tendency is still present for all three cases (SM1-SM3). The periodic nature of the average concentration plots indicates that none of the three solutions is able to negate the influence of the breathing process in regards to CO_2 accumulation. The highest accumulation is, rather unintuitively, found in the SM2 case with frontal PV, showing an increase of about 30 ppm of CO_2 over 20s. The increase for the SM1 case is about 28 ppm, while for SM3 average CO_2 levels increase by 25 ppm over 20s. Despite the presence of the PV diffuser in models SM2 and SM3 we can see that for the latter case the CQ CO_2 levels decrease in comparison to SM1, while for the former, an increase is observed. This highlights the significant influence of the PV system's position.

An interesting observation was made regarding the SM2 case. Upon investigating the MP plane of SM2 at time instants t_2 and t_3 (Fig. 9c and d), a design flaw is found for the frontal PV solution in the present case. Because of the particular geometry of the human occupant (the

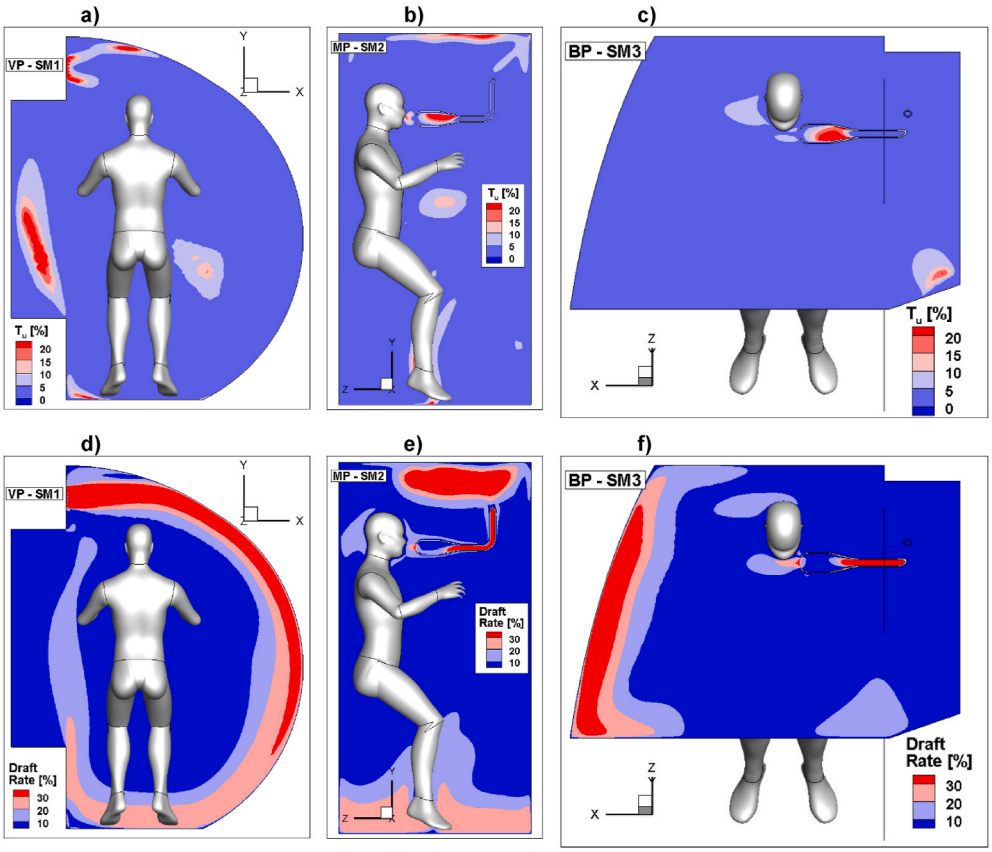

Fig. 11. Turbulence intensity (a–c) and Draft rate (*d*–f) comparison between the VP in SM1, the MP in SM2 and the BP in SM3.

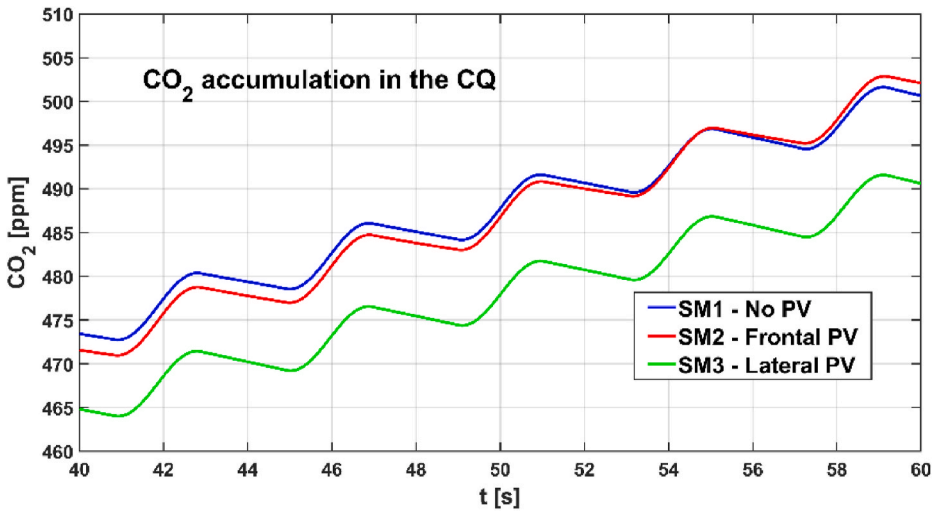

Fig. 12. Average CO_2 concentration in the CQ comparison between different ventilation setups: CFF ventilation (SM1); CFF and frontal PV ventilation (SM2); CFF and lateral PV ventilation (SM3).

positioning of its nostrils, detailed in previous work [15]) and the proximity of the PV diffuser, the breath pollutes the PV diffuser with CO_2 during exhalation. At time t_2 representing the end of the exhalation Fig. 13a shows the CO_2 concentration in and around the PV diffuser, which in addition to having the supply air polluted, acts as a barrier for the breath, preventing the CO_2 from dispersing in the CQ. At peak inhalation (t_3) the PV diffuser has yet to replace the CO_2 accumulated inside it with fresh air as can be seen in Fig. 13b. However, the average CO_2 level in the CQ is not an accurate indicator of the CO_2 inhaled by the occupant from the BZ, which is the next point of interest for the present study.

This phenomenon can be explained by considering the average velocity values of the PV supply jet and the occupant's breath. The average PV jet velocity at the diffuser exit is 0.4 m/s, based on its flow rate of 1 m^3/h and equivalent diameter of 3 cm. Similarly, the average exhalation velocity based on the velocity sine function is 3.5 m/s. This velocity difference explains the exhaled air penetrating the PV diffuser.

Because the purpose of the PV system was to supply fresh air to the occupant, it is clear that the frontal PV solution is incapable of fulfilling its basic scope. Not only that, but it appears to worsen the air quality in the BZ of the occupant. For this reason, model SM2, covering the frontal PV solution will not be studied further and only SM1 and SM3 will be compared below.

Previous work concerning the CO_2 accumulation in the CQ [15] has defined a breathing zone (BZ) for the occupant, by applying Fast Fourier Transforms to the periodic human breath. Since the present study uses the same breathing function as [15], it follows that the BZ previously defined is applicable in the present case as well. The evaluation of CO_2 levels in the BZ between SM1 and SM3 is the final part of this study. The first objective is a visual comparison of the BZ CO_2 levels to see if the impact of the lateral PV system is noticeable, while the second objective is a quantitative comparison of the CO_2 in the BZ during a full breathing cycle.

Fig. 14 superposes the BZ defined in Ref. [15] over the BP and the MP of SM1 and SM3 cases (Fig. 14$a_{1/2}$ for SM1 and Fig. 14$b_{1/2}$ for SM3). To recall the results of [15], in the yellow zone marked full-cycle influence both the exhalation and the inhalation is strongly felt, while in the zone marked with a dashed black line (marked half-cycle influence) the exhalation is predominant. The BP of SM1 and SM3 (Fig. 14a_1 and b_1) at the end of the exhalation (t_2) shows for both cases a tendency of the exhaled air to be entrained towards the curved wall (to the left of the image from the perspective of Fig. 14). This entrainment is expected and is caused by the general ventilation jet which follows the path of the curved CQ wall. However, the influence of the lateral PV solution is felt in Fig. 14b_1 as the breathing jet is visibly displaced from the BZ.

Looking at the MP of SM1 (Fig. 14a_2), CO_2 concentrations over 2000 ppm are seen almost up to the far end of the BZ, with no point dropping below 1600 ppm. In contrast, the MP of SM3 (Fig. 14b_2) shows notably lower CO_2 concentrations in the BZ with values over 800 ppm being present only for half the BZ length, and values over 2000 ppm extending

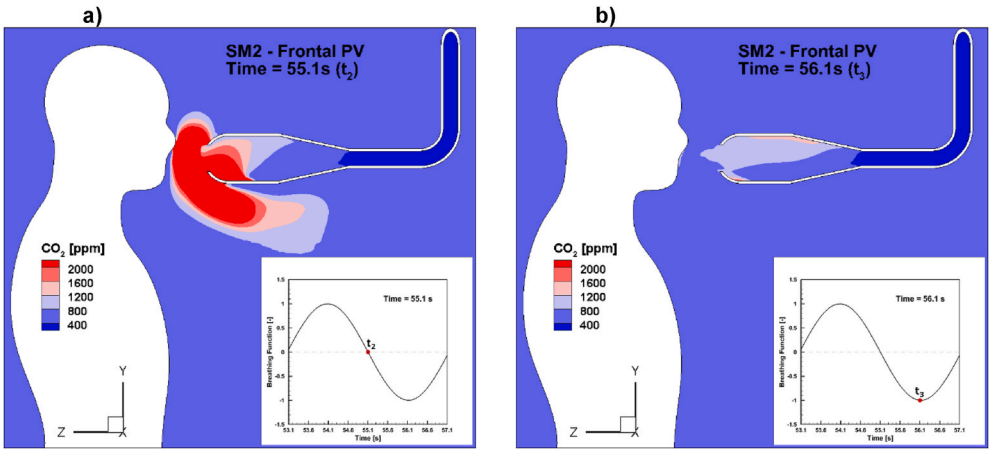

Fig. 13. Interaction of breath dynamics and the PV diffuser for case SM2 in MP at time instants t2 (a) and t4 (b).

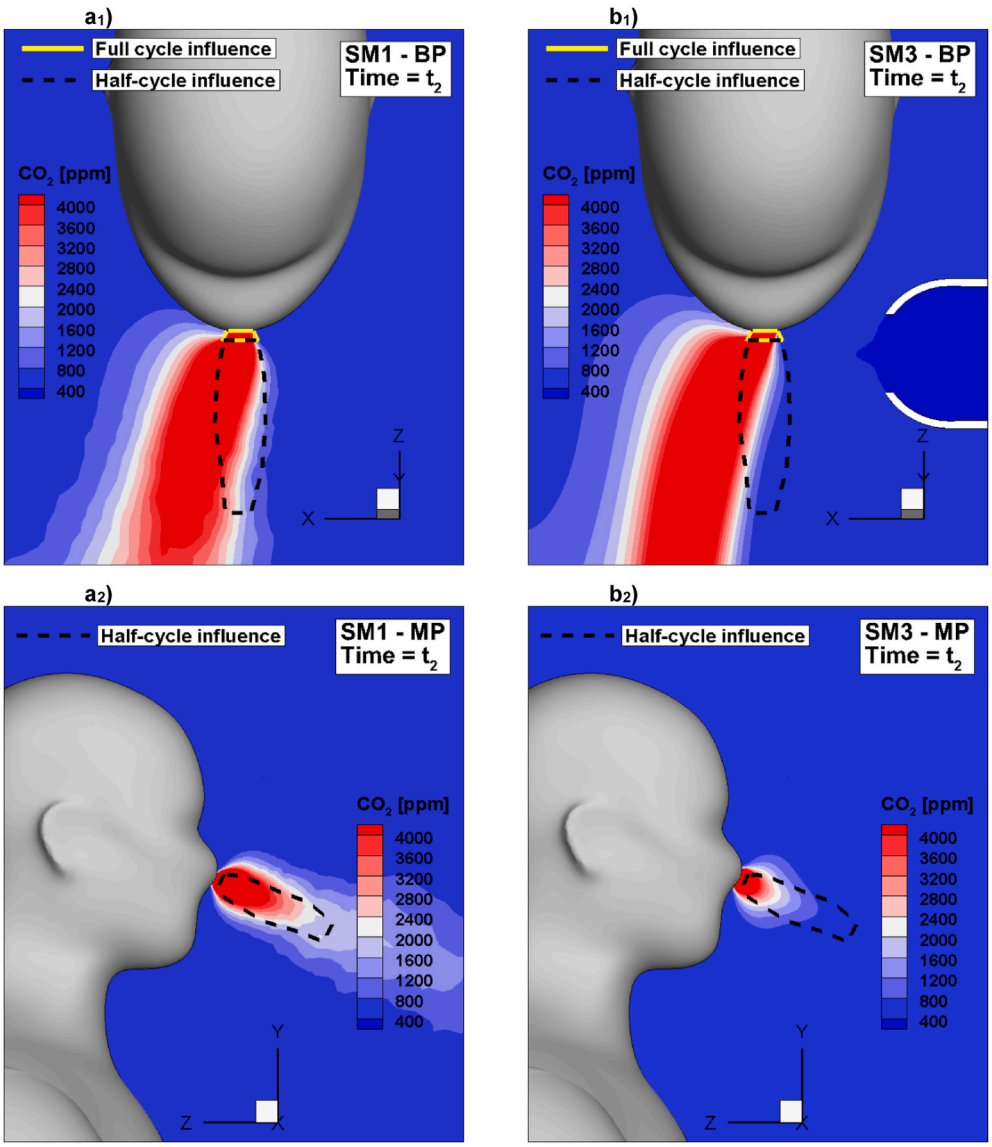

Fig. 14. CO_2 accumulation in the BZ for cases: SM1 (a) and SM3 (b) models in planes MP (1) and BP (2).

only up to a quarter of its length. The PV jet is not strong enough to completely displace the exhaled CO_2 during the exhalation process, but its influence is clear and it has the potential to completely remove CO_2 for the BZ during inhalation more quickly than the general ventilation system could by itself. The conclusion drawn from the fact that in Fig. 14a_1 the jet is entrained towards the curved wall of the CQ, is that the CO_2 will eventually be removed from the BZ due to the recirculation inside the CQ. The question is how much of the CO_2 reduction in the BZ is caused by the ventilation system (PV or otherwise) supplying fresh air, and what is the re-inhaled fraction of CO_2 for the occupant.

A quantitative evaluation of CO_2 levels in the BZ was performed over the course of an entire breathing cycle (exhalation and inhalation), to fully illustrate the differences between the model using only the general ventilation system (SM1) and the one using the lateral PV solution as well (SM3). CO_2 concentrations vary in the BZ by a significant amount due to the exhaled air having a concentration 100 times greater than the ambient air (40000 ppm as opposed to ~400). Representing the CO_2 over a breathing cycle in the BZ via concentrations would generate vastly different scales between exhalation and inhalation rendering evaluation difficult. For this reason, the quantitative evaluation of CO_2 will be presented in units of volume (ml) as opposed to concentrations (ppm). This is done easily by integrating the concentration values over the volume of the BZ.

Fig. 15 shows the volume of CO_2 [ml] present in the BZ over the course of a breathing cycle beginning at 53.05s into the simulation and ending at 57.1s (total duration of ~4s). The CO_2 volume is presented for both the SM1 (long dashed line) and SM3 (full line) cases. The breath velocity at the nostrils is plotted on the second Y axis, in a dashed and dotted line, common to the two cases. CO_2 and velocity values during the exhalation part of the breathing cycle are colored in red while those during the inhalation cycle are colored in blue.

The values of CO_2 in the BZ at the start and end of the breathing process as well as at the start of the inhalation were extracted from Fig. 15 and presented in Table 3. At the start of the inhalation phase the CO_2 content in the BZ with the lateral PV solution is almost three times lower than the CO_2 content without it. The difference in CO_2 volume in the BZ between the start of the breathing cycle and its end is almost nil (of the order E−05), indicating that the general ventilation solution is capable of clearing the exhaled CO_2 from the BZ even without the PV system. Despite this fact, the lower CO_2 volumes during the breathing cycle highlighted in Fig. 15 for SM3 indicate that there is a possibility that in this case the occupant inhales less CO_2 during an inhalation cycle.

To evaluate the quantity of inhaled CO_2 between the SM1 and SM3 cases, the Intake Fraction (IF) is used. The Intake Fraction represents the

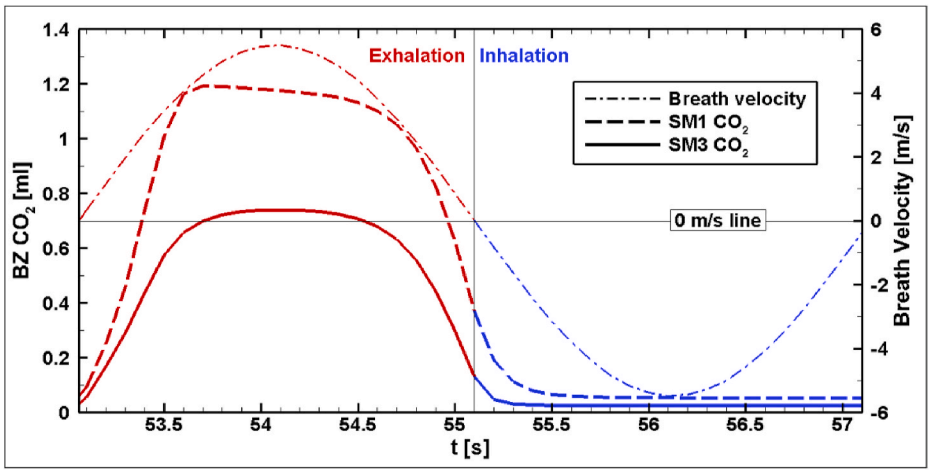

Fig. 15. Comparison of CO_2 variation in the BZ during one breathing cycle (exhalation and inhalation) for SM1 (no PV) and SM3 (lateral PV).

Table 3
Quantitative data of CO_2 volume in the BZ extracted from Fig. 15 for SM1 and SM3.

	SM1	SM3
Initial CO_2 volume in the BZ [ml] (t = 53.1s)	0.05	0.02
CO_2 content in the BZ at the start of the inhalation [ml]	0.31	0.11
Final CO_2 volume in the BZ [ml] (t = 57.1s)	0.05	0.02
ΔCO_2 volume in the BZ [ml]	**~0**	**~0**

quantity of an inhaled pollutant, normalized by the quantity of pollutant emitted [40]. The IF in the present study is expressed through Equation (2) where Q [m^3/s] is the flow rate through the nostrils, and $MFCO_2$ [-] is the average CO_2 mass fraction on the nostrils and ρ_{air} [kg/m^3] is the average density of the air on the nostrils.

$$IF = \frac{\int_{t_0}^{t_2} MFCO_2(t)\cdot Q_{inhaled}(t)\cdot\rho_{air}(t)\,dt}{\int_{t_2}^{t_4} MFCO_2(t)\cdot Q_{exhaled}(t)\cdot\rho_{air}(t)\,dt} \quad (2)$$

The Intake Fractions resulted from Equation (2) for the SM1 and SM3 cases are presented in Table 4. The results indicate that there is a difference in intake fractions between the two models, with the occupant of SM3 inhaling 8% less CO_2 than the occupant of the SM1 case.

The results so far indicate that the lateral PV system is a simple addition to the general ventilation system that can reduce the quantity of CO_2 inhaled by the CQ occupants. For the time period evaluated in the present study (60s) the difference between the lateral PV system and using solely the general ventilation is not overwhelming. However, recalling the results shown in Fig. 12, there is in both cases an accumulation of CO_2 in the CQ. It is likely that given enough time the CQ air becomes more and more charged with CO_2 leading to ever increasing quantities of CO_2 inhaled by the occupant. In such a case the lateral PV system has the advantage of supplying fresh air directly to the occupant's breathing zone as opposed to ventilating it via the air recirculation in the CQ (as the general ventilation system does). The magnitude and efficiency of the lateral PV solution over longer periods of time warrants further investigation.

Table 4
Intake Fraction values for the SM1 and SM3 cases.

	SM1	SM3
IF	0.0122	0.0112

4.4. Limitations

The limitations of the current PV solution concern their positioning relative to the CQ occupant. Astronauts on the ISS have a sleeping bag attached to the CQ wall which they can use keeping their position relatively fixed, but if they opt not to use this bag, they could float out of the PV influence area. To combat this phenomenon a portable PV solution warrants future study. Additionally, dust accumulation in the PV ducts could prove to be an issue. Finally, the numerical results offer insight into the general behavior of the ventilation system for an average occupant, but in reality physiological differences between individual occupants could provide different real-world results.

5. Conclusion

The present paper investigated the possibility of adding a personalized ventilation (PV) solution to a new configuration of the general ventilation system of the CQ aboard the ISS. The implementation of two PV solutions were evaluated numerically, based on previously validated work and models. The CFD's capabilities to reproduce the development of the PV jet was validated by comparing the numerical results to experimental measurements of velocity fields at different distances between the PV diffuser and a model of the human occupant. The experimental velocity fields were measured with a hot-sphere anemometer, covering a grid of measurement points in a plane in front of the diffuser. Numerical validation via experimental results was considered satisfactory.

Two personal ventilation solutions were proposed: the first had the PV diffuser installed in front of the human occupant of the CQ at a distance of $2D_e$ from the face; the second solution had the PV diffuser placed laterally, perpendicular to the breathing jet, this second solution was aimed at the breathing zone of the occupant and situated $2D_e$ away, the same distance as in the first case. The two PV solutions were compared with a case featuring only the general ventilation system and the human occupant. Unsteady numerical simulations were performed with a time step of 0.05s over the course of 1 min, during which time the human occupant acted as a source of CO_2 in the CQ. Human CO_2 generation was caused by the breath, which was simulated as a time-dependent velocity sine function with a breathing frequency of 14.7 breaths/min (resulted from previous experimental measurements).

The two PV solutions were found to not significantly impact either the global air distribution in the CQ, not the comfort sensation of the occupant. Investigations of CO_2 accumulation revealed that in all three cases an overall accumulation was still found in the CQ. During these initial investigations it was found that the placement of the frontal PV diffuser was too close to the occupant's face and acted as a barrier

preventing the exhaled CO_2 from dispersing, worsening the accumulation. The frontal PV solution was thus discarded and future recommendations for such solutions are to place them further away from the occupant's face associated with an eventual increase in PV jet flow rate to compensate for the increased distance.

The lateral PV solution proved to be efficient, showing reduced CO_2 content in the breathing zone of the occupant across the whole breathing cycle. Although both the lateral PV solution and the general ventilation system alone were capable of removing the exhaled CO_2 from the BZ across a breathing cycle, closer inspection revealed an 8% reduction in inhaled CO_2 over each breath in the case of the lateral PV system. Because the phenomenon of overall CO_2 accumulation in the CQ is present in both cases, ambient CO_2 levels are bound to rise. The capability of the PV system to supply fresh air directly to the BZ could be invaluable when simulating longer periods of time and warrants further investigation.

Declaration of competing interest

The authors declare that they have no known competing financial interests or personal relationships that could have appeared to influence the work reported in this paper.

Acknowledgements

This work was supported by a "Presidency" scholarship from the University of Rennes 1, for which the authors are grateful.

This work was also supported by the grant of the Romanian Space Agency ROSA STAR-CDI-C3-2016-577.

References

[1] Nasa, National aeronautics and space administration, Human Integration Design Handbook (2010) 1–27, https://doi.org/10.4135/9781412939591.n797. Spaceflight (Lond).
[2] J.T. James, The headache of carbon dioxide exposures, SAE Tech. Pap. (2007), https://doi.org/10.4271/2007-01-3218.
[3] S. Fairburn, S. Walker, 'Sleeping with the stars' – the design of a personal crew quarter for the international space station, in: 31st Int. Conf. Environ. Syst., 2001, https://doi.org/10.4271/2001-01-2169.
[4] J.L. Broyan, M.A. Borrego, J.F. Bahr, International space station USOS crew quarters development, in: 38th Int. Confeence Environ. Syst., 2008, https://doi.org/10.4271/2008-01-2026.
[5] J. Broyan, D. Welsh, S. Cady, International space station crew quarters ventilation and acoustic design implementation, 40th Int. Conf. Environ. Syst. (2010) 1–16, https://doi.org/10.2514/6.2010-6018.
[6] T.P. Schlesinger, B.R. Rodriguez, International space station crew quarters on-orbit performance and sustaining activities, Int. Conf. Environ. Syst. (2013) 1–9, https://doi.org/10.2514/6.2013-3515.
[7] J.L. Broyan Jr., M.A. Borrego, J.F. Bahr, International space station United States operational segment crew quarters on -orbit vs. Design performance comparison, SAE Int. J. Aerosp. 4 (2011) 98–107, https://doi.org/10.4271/2009-01-2367.
[8] J.T. James, V.E. Meyers, W. Sipes, R.R. Scully, C.M. Matty, Crew Health and Performance Improvements with Reduced Carbon Dioxide Levels and the Resource Impact to Accomplish Those Reductions, 2011, pp. 1–7.
[9] D. Law J, S. Watkins, W.S. Alexander, J. Law, In-flight carbon dioxide exposures and related symptoms: associations, susceptibility and operational implications, NASA Tech. Rep. (2010) 1–21, https://doi.org/10.3390/e21060541.
[10] R.M. Bagdigian, N. Marshall, S. Flight, International Space Station Environmental Control and Life Support System Mass and Crewtime Utilization in Comparison to a Long Duration Human Space Exploration Mission, 2015.
[11] C.M. Matty, Overview of carbon dioxide control issues during international space station/space shuttle joint docked operations, in: 40th Int. Conf. Environ. Syst., vol. 2, 2010, pp. 1–9, https://doi.org/10.2514/6.2010-6251.
[12] F. Parker, R. West, BIOASTRONAUTICS DATA BOOK, second ed., NASA, 1973. https://ntrs.nasa.gov/api/citations/19730006364/downloads/19730006364.pdf.
[13] J. Pantelic, S. Liu, L. Pistore, D. Licina, M. Vannucci, S. Sadrizadeh, A. Ghahramani, B. Gilligan, E. Sternberg, K. Kampschroer, S. Schiavon, Personal CO2 cloud: laboratory measurements of metabolic CO2 inhalation zone concentration and dispersion in a typical office desk setting, J. Expo. Sci. Environ. Epidemiol. 30 (2020) 328–337, https://doi.org/10.1038/s41370-019-0179-5.
[14] C. Son, J. Zapata, C. Lin, Investigation of airflow and accumulation of carbon dioxide in the service module crew quarters, Int. Conf. Environ. Syst. (2002) 2341, https://doi.org/10.4271/2002-01-2341.
[15] M.R. Georgescu, A. Meslem, I. Nastase, Accumulation and spatial distribution of CO2 in the astronaut's crew quarters on the International Space Station, Build. Environ. 185 (2020) 107278, https://doi.org/10.1016/j.buildenv.2020.107278.
[16] M.R. Georgescu, A. Meslem, I. Nastase, M. Sandu, Numerical and experimental study of the International Space Station crew quarters ventilation, J. Build. Vent. 41 (2021), https://doi.org/10.1016/j.jobe.2021.102714.
[17] M.R. Georgescu, A. Meslem, I. Nastase, L. Tacutu, An alternative air distribution solution for better environmental quality in the ISS crew quarters, Accept. Int. J. Vent (2021).
[18] A.K. Melikov, Human body micro-environment: the benefits of controlling airflow interaction, Build. Environ. 91 (2015) 70–77, https://doi.org/10.1016/j.buildenv.2015.04.010.
[19] A. Makhoul, K. Ghali, N. Ghaddar, Desk fans for the control of the convection flow around occupants using ceiling mounted personalized ventilation, Build. Environ. 59 (2013) 336–348, https://doi.org/10.1016/j.buildenv.2012.08.031.
[20] Z. Bolashikov, A. Melikov, M. Krenek, Control of the free convective flow around the human body for enhanced inhaled air quality: application to a seat-incorporated personalized ventilation unit, HVAC R Res. 16 (2010) 161–188, https://doi.org/10.1080/10789669.2010.10390899.
[21] Z.D. Bolashikov, A.K. Melikov, Methods for air cleaning and protection of building occupants from airborne pathogens, Build. Environ. 44 (2009) 1378–1385, https://doi.org/10.1016/j.buildenv.2008.09.001.
[22] A.K. Melikov, V. Dzhartov, Advanced air distribution for minimizing airborne cross-infection in aircraft cabins, HVAC R Res. 19 (2013) 926–933, https://doi.org/10.1080/10789669.2013.818468.
[23] Z. Bolashikov, L. Nikolaev, A.K. Melikov, J. Kaczmarczyk, P. Fanger, Personalized ventilation: air terminal devices with high efficiency, in: Proc. Heal. Build., 2003, pp. 850–855. Singapore.
[24] J. Niu, N. Gao, M. Phoebe, Z. Huigang, Experimental study on a chair-based personalized ventilation system, Build. Environ. 42 (2007) 913–925, https://doi.org/10.1016/j.buildenv.2005.10.011.
[25] Z.D. Bolashikov, Advanced Methods for Air Distribution in Occupied Spaces for Reduced Risk from Air-Borne Diseases and Improved Air Quality, Technical University of Denmark, Department of Civil Engineering, Kgs. Lyngby, Denmark, 2010.
[26] A. Meslem, I. Nastase, F. Allard, Passive mixing control for innovative air diffusion terminal devices for buildings, Build. Environ. 45 (2010) 2679–2688, https://doi.org/10.1016/j.buildenv.2010.05.028.
[27] I. Nastase, A. Meslem, Vortex dynamics and mass entrainment in turbulent lobed jets with and without lobe deflection angles, Exp. Fluid 48 (2010) 693–714, https://doi.org/10.1007/s00348-009-0762-y.
[28] A. Meslem, M. El Hassan, I. Nastase, Analysis of jet entrainment mechanism in the transitional regime by time-resolved PIV, J. Vis. 14 (2011) 41–52, https://doi.org/10.1007/s12650-010-0057-7.
[29] I. Nastase, A. Meslem, P. Gervais, Primary and secondary vortical structures contribution in the entrainment of low Reynolds number jet flows, Exp. Fluid 44 (2008) 1027–1033, https://doi.org/10.1007/s00348-008-0488-2.
[30] I. Nastase, A. Meslem, I. Vlad, I. Colda, Lobed grilles for high mixing ventilation - an experimental analysis in a full scale model room, Build. Environ. 46 (2011) 547–555, https://doi.org/10.1016/j.buildenv.2010.08.008.
[31] Z. Bolashikov, A. Melikov, M. Spilak, I. Nastase, A. Meslem, Improved inhaled air quality at reduced ventilation rate by control of airflow interaction at the breathing zone with lobed jets, HVAC R Res. 20 (2014) 238–250, https://doi.org/10.1080/10789669.2013.864919.
[32] J. Kaczmarczyk, A. Melikov, Z. Bolashikov, L. Nikolaev, P.O. Fanger, Human response to five designs of personalized ventilation, HVAC R Res. 12 (2006) 367–384, https://doi.org/10.1080/10789669.2006.10391184.
[33] Z. Bolashikov, A. Melikov, M. Spilak, Experimental investigation on reduced exposure to pollutants indoors by applying wearable personalized ventilation, HVAC R Res. 19 (2013) 385–399, https://doi.org/10.1080/10789669.2013.784645.
[34] A. Melikov, T. Sakoi, S. Kolencikova, Impact of air movement on eye symptoms, in: Proc. 11th REHVA World Congr. 8th Int. Conf. Indoor Air Qual. Vent, Energy Conserv. Build., Prague, 2013.
[35] E.M. Smirnov, N.G. Ivanov, D.S. Telnov, C.H. Son, CFD modelling of cabin air ventilation in the international space station: a comparison of RANS and LES data with test measurements for the Columbus module, Int. J. Vent. 5 (2006) 219–227, https://doi.org/10.1080/14733315.2006.11683739.
[36] C.H. Son, V.K. Aksamentov, E.M. Smirnov, N.G. Ivanov, D.S. Telnov, CFD modeling for Ventilation : a method for Reynolds-averaged Navier-Stokes (RANS) data correlation, in: 17th Air-Conditioning Vent. Conf., 2006. Prague.
[37] F. Bode, A. Meslem, C. Patrascu, I. Nastase, Flow and wall shear rate analysis for a cruciform jet impacting on a plate at short distance, Prog. Comput. Fluid Dynam. Int. J. 20 (2020) 169–185, https://doi.org/10.1504/PCFD.2020.107276.
[38] International Organization for Standardization, ISO 7730: Ergonomics of the Thermal Environment—Analytical Determination and Interpretation of Thermal Comfort Using Calculation of the PMV and PPD Indices and Local Thermal Comfort Criteria, 2013.
[39] ANSI/ASHRAE, Standard 55/2010 Thermal Enviornmental Conditions for Human Occupancy, 2010.
[40] A.K. Melikov, Z.T. Ai, D.G. Markov, Intermittent occupancy combined with ventilation: an efficient strategy for the reduction of airborne transmission indoors, Sci. Total Environ. 744 (2020), https://doi.org/10.1016/j.scitotenv.2020.140908.